Am J Cancer Res 2026;16(1):141-158
www.ajcr.us /ISSN:2156-6976/ajcr0169060

Original Article

Desmoglein-2 promotes the proliferation and invasion of lung adenocarcinoma cells by inhibiting anoikis through the activation of the integrin beta-1/focal adhesion kinase signaling pathway

Xuelin Zhang[1,3], Man Su[2], Fu Niu[1], Lei Sun[3], Chang Liu[3], Bo Wang[3], Meina Hu[3], Zhigang Cai[1]

[1]The First Department of Pulmonary and Critical Care Medicine, The Second Hospital of Hebei Medical University, Shijiazhuang 050000, Hebei, China; [2]Department of Endocrinology, The Third Hospital of Shijiazhuang, Shijiazhuang 050000, Hebei, China; [3]The First Department of Pulmonary and Critical Care Medicine, The Third Hospital of Shijiazhuang, Shijiazhuang 050000, Hebei, China

Received September 28, 2025; Accepted January 3, 2026; Epub January 15, 2026; Published January 30, 2026

Abstract: Patients with advanced lung adenocarcinoma often develop metastasis and recurrence, leading to treatment failure. Anoikis resistance is a key step in tumor metastasis. Desmoglein-2 (DSG2) plays an important role in several cancers; however, its role in lung adenocarcinoma and its relationship to anoikis remain unclear. In this study, we aimed to investigate whether DSG2 regulates proliferation, invasion, and anoikis in lung adenocarcinoma cells and to explore the underlying mechanism. We analyzed DSG2 expression in lung cancer tissues and cells using online databases, examining the effects of DSG2 knockdown and overexpression on proliferation, invasion, and anoikis in lung adenocarcinoma cell models. Furthermore, we examined whether DSG2 functions through the integrin β1/focal adhesion kinase (FAK) signaling pathway and evaluated the effects of the integrin β1 agonist Pyrintegrin. DSG2 was highly expressed in lung adenocarcinoma tissues and cells and was associated with poor prognosis. DSG2 knockdown inhibited proliferation and invasion and promoted anoikis, whereas DSG2 overexpression increased invasion and proliferation and suppressed anoikis. Mechanistic analysis revealed that DSG2 activated the integrin β1/FAK signaling pathway. Pyrintegrin reversed the inhibitory effects of DSG2 knockdown on lung adenocarcinoma cells. DSG2 inhibits anoikis in lung adenocarcinoma cells by activating the integrin β1/FAK signaling pathway, thereby promoting cell proliferation and invasion.

Keywords: Lung adenocarcinoma, DSG2, anoikis, integrin β1/FAK signaling pathway, cell invasion

Introduction

Lung adenocarcinoma (LUAD), the most prevalent form of non-small cell lung cancer, accounts for over 40% of all lung cancer cases and continues to show high global incidence and mortality rates worldwide [1, 2]. Despite advances in targeted therapy and immunotherapy, patients with LUAD still experience a low 5-year survival. Those with advanced-stage disease are particularly prone to metastasis and recurrence, which often lead to treatment failure [3]. For patients with LUAD, tumor metastasis remains the leading cause of death. Anoikis resistance, a critical step in the metastatic process, allows tumor cells to survive and spread after detaching from the primary site [4, 5]. However, the development of effective targeted therapies is hindered by limited research on anoikis and the incomplete elucidation of its molecular mechanisms. Thus, identifying how LUAD cells evade anoikis is essential for clarifying the molecular drivers of metastasis and creating innovative therapeutic approaches.

Anoikis is a form of programmed cell death that occurs when cells lose contact with each other or detach from the extracellular matrix (ECM) [6]. Under normal conditions, anoikis acts as a protective mechanism that prevents abnormal cells from spreading. Tumor cells, however, resist anoikis through various mechanisms, enabling them to survive and colonize distant organs during metastasis [7, 8]. Studies show

that LUAD cells significantly enhance resistance by regulating signaling pathways such as transforming growth factor β1 (TGFβ1)/integrin β3 and focal adhesion kinase (FAK)/Src or by modulating molecules including B-cell lymphoma 2 (Bcl-2) family proteins and integrins [9-11]. Anoikis resistance is closely linked to the invasive and migratory abilities of tumor cells. For instance, anoikis-resistant cells often display enhanced epithelial-mesenchymal transition characteristics and increased ECM degradation [12, 13]. Therefore, clarifying the molecular mechanism of anoikis resistance is essential for understanding LUAD metastasis and identifying new therapeutic targets to inhibit tumor spread.

Desmoglein-2 (DSG2), a key member of the cadherin family, is predominantly involved in the formation and maintenance of intercellular adhesive junctions [14]. Recent studies show that DSG2 contributes to the development of several cancers, and abnormal DSG2 expression is significantly associated with tumor invasion, metastasis, and proliferation [15-17]. For instance, in gastric cancer, DSG2 promotes tumor progression by regulating the epidermal growth factor receptor/AKT signaling pathway [18]. Furthermore, DSG2 reduces the therapeutic efficacy of gemcitabine [19] and is predicted to have diagnostic value in lung cancer [20]. However, the role of DSG2 in LUAD and its relationship with anoikis remain unclear. Considering its central role in cell adhesion and signal transduction, along with its tumor-promoting effects in other cancers, DSG2 may be an important factor that enables LUAD cells to resist anoikis and promote metastasis. Consequently, investigating DSG2-mediated anoikis resistance in LUAD is essential for identifying new metastatic mechanisms and providing a theoretical foundation for developing DSG2-targeted therapeutic strategies. Therefore, we aimed to investigate whether DSG2 regulates proliferation, invasion, and anoikis in LUAD cells and to explore the underlying mechanism.

Materials and methods

Differential expression and prognosis analysis of DSG2 in the TCGA-LUAD cohort

We obtained LUAD data from The Cancer Genome Atlas (TCGA, https://www.cancer.gov/ccg/research/genome-sequencing/tcga). Samples were divided into normal (n = 347) and tumor (n = 483) groups, and DSG2 expression levels were compared between these groups. Overall survival curves for the two patient groups were plotted using the Kaplan-Meier method, and the log-rank test was used to assess significant differences [21]. The relative expression levels of DSG2 in several LUAD cell lines were retrieved from the CCEL (http://gepia2.cancer-pku.cn/#analysis).

Weighted gene co-expression network analysis of the TCGA-LUAD dataset

To identify co-expression modules associated with DSG2 and their enriched biological functions, we performed a WGCNA. The analysis used the TCGA-LUAD dataset, comprising 40 LUAD samples and 40 control samples. Raw gene expression data were provided in log2-transcripts per million format. We applied stringent gene filtering: (1) genes with zero expression across all samples were removed; (2) low-expression genes below the 25th percentile were excluded; (3) genes with low variability (coefficient of variation below the 10th percentile) were filtered out; and (4) genes with missing values in more than 20% of samples were discarded. Following preprocessing, the data were transposed into a sample-by-gene matrix and quality-checked using the WGCNA function goodSamplesGenes. At the sample level, hierarchical clustering (Euclidean distance, average linkage) detected outlier samples. A dynamic cut height (95th percentile) was applied to remove abnormal samples, retaining core samples for subsequent analysis.

The pickSoftThreshold function was used to test power values from 1 to 30, and the minimum power that achieved a scale-free topology fit index (R^2) ≥ 0.8 was selected as the soft threshold. The gene co-expression network was constructed using a signed network type, and the topological overlap matrix quantified gene similarity. Co-expression modules were identified using the dynamic tree-cutting method, and modules with similarity greater than 0.25 were merged. The Pearson correlation between MEs and the clinical trait (LUAD/control) was calculated, and statistical significance (*P*-value) was evaluated. DSG2 was mapped to the BLACK module, and all genes in this mod-

ule were extracted for subsequent functional analysis.

Gene functional enrichment analysis

We performed functional enrichment analysis, including GO and KEGG analyses, on genes within the DSG2-containing module. The clusterProfiler package was used to convert gene symbols to ENTREZ IDs. GO analysis covered Biological Process, Cellular Component, and Molecular Function categories. KEGG analysis was based on the human genome (hsa). Statistical significance was set at P-value < 0.05 with Benjamini-Hochberg correction.

Survival analysis

To validate the prognostic significance of DSG2 in LUAD, we used the independent dataset GSE68465, which includes gene expression and clinical survival data from 442 LUAD samples. DSG2 expression values were extracted and merged with clinical information, including survival time (in months) and survival status (death = 1, alive = 0). To minimize bias, interfering samples were excluded. Subsequently, the optimal cut-point for DSG2 expression was determined using the surv_cutpoint function, dividing samples into high- and low-expression groups. Kaplan-Meier curves were plotted, and the log-rank test assessed differences between groups. Furthermore, a Cox proportional hazards model was constructed to calculate the hazard ratio (HR) and its 95% confidence interval.

Cell culture

Human LUAD cell lines NCI-H3255, NCI-H2347, and NCI-H522 were obtained from Shanghai Jinyuan Biotechnology Co., Ltd. (https://ssrcc.com.cn/). Qingqi Biotechnology Development Co., Ltd. provided the LUAD cell lines A549 and A427, as well as the normal lung epithelial cell line BEAS-2B (http://www.bluefcell.com/gsjj, Shanghai, China). Cells were cultured in RPMI 1640 medium (C2721; Shanghai Biyuntian Biotechnology Co., Ltd., Shanghai, China) supplemented with 10% fetal bovine serum (FBS; C0226; Shanghai Biyuntian Biotechnology Co., Ltd., Shanghai, China) and 1% penicillin-streptomycin solution (C0222; Shanghai Biyuntian Biotechnology Co., Ltd., Shanghai, China). Cultures were maintained in a 37°C, 5% CO_2 incubator (51023126, Thermo Fisher Scientific, China). All cell lines were authenticated by an expert prior to use and confirmed to be free of mycoplasma contamination.

Cell transfection

NCI-H2347 and NCI-H522 LUAD cells were collected during the exponential growth phase. Cells were treated with 3 mL of trypsin solution (C0202; Shanghai Biyuntian Biotechnology Co., Ltd., Shanghai, China) and incubated for 2 min, then centrifuged at 1200×g for 3 min and resuspended in 3 mL of RPMI 1640 medium. Cells (1×10^5 per well) were seeded into the six-well plates and incubated overnight. The medium was replaced the following day with a mixture of Lipo 3000 transfection reagent (L3000075; Thermo Fisher Scientific) and interfering RNA sequences or overexpression plasmids. Cells were cultured for 3 h in serum-free RPMI 1640 medium, after which RPMI 1640 containing serum was added, and incubation continued for 48 h. NCI-H2347 cells were divided into three groups: si-NC, si-DSG2-1, and si-DSG2-2. NCI-H522 cells were divided into vector and oe-DSG2 (overexpression of DSG2) groups. The sequences of siRNA and overexpression plasmids are listed in Supplementary Table 1. Pyrintegrin (HY-13306; MedChemExpress, China), a β1-integrin agonist [22], was used to verify DSG2 regulation of the integrin β1/FAK signaling pathway; cells were divided into si-NC, si-DSG2-1, and si-DSG2-1 + Pyrintegrin groups. ATN-161 (HY-13535; MedChemExpress, China), an integrin β1/FAK signaling pathway inhibitor, was applied in experiments dividing cells into vector, oe-DSG2, and oe-DSG2 + ATN-161 groups.

Observation of anoikis cell morphology

DSG2-knockdown NCI-H2347 cells and DSG2-overexpressing NCI-H3255 LUAD cells were used. After cell counting, cells were seeded at 1×10^5 per well in six-well ultra-low attachment plates (FULA061; Shanghai Biyuntian Biotechnology Co., Ltd.) and incubated overnight. Morphological changes associated with anoikis were observed under a microscope (AMF70-00HCA; Thermo Fisher Scientific).

CCK-8 assay

DSG2-knockdown NCI-H2347 cells and DSG2-overexpressing NCI-H3255 LUAD cells were seeded at 2×10^3 cells per well in 96-well

plates and incubated overnight. Ten microliters of CCK-8 solution (C0039; Shanghai Biyuntian Biotechnology Co., Ltd.) was added to each well, and the plates were incubated for 3 h. Absorbance was measured at 450 nm to calculate cell viability:

Cell viability (%) = (optical density [OD] value of experimental group - OD value of blank control group)/(OD value of control group - OD value of blank control group).

EDU assay

DSG2-knockdown NCI-H2347 cells and DSG2-overexpressing NCI-H3255 LUAD cells were used. Cells were seeded at 1×10^5 in six-well plates and incubated overnight. The next day, cells were treated with 10 μmol/L EdU working solution (C0078S; Shanghai Biyuntian Biotechnology Co., Ltd.) and incubated for 2 h. Tissue and cell fixatives (P0099; Shanghai Biyuntian Biotechnology Co., Ltd.) were added, and samples were incubated for an additional 4 h. Images were captured using a fluorescent microscope, and the proportion of EdU-positive cells was calculated using ImageJ, version 1.5.2a.

Transwell assay

RPMI 1640 medium was mixed with BD Matrigel (354248; Corning Incorporated, China) at an 8:1 ratio. Fifty microliters of the mixture were added to the upper chamber of a Transwell insert and incubated for 4 h. DSG2-knockdown NCI-H2347 cells and DSG2-overexpressing NCI-H3255 LUAD cells were used. The upper Transwell chamber was seeded with 1×10^5 cells in 100 μL medium. The lower chamber contained RPMI 1640 medium with 20% FBS and was incubated for 16 h. Following incubation, cells were washed with phosphate-buffered saline (PBS), and the medium was removed. The lower chamber was fixed with 500 μL of tissue and cell fixative for 30 min, followed by staining with 500 μL of 0.1% crystal violet (Y268093; Shanghai Biyuntian Biotechnology Co., Ltd.) was added and incubated for 30 min. Images were captured from five randomly chosen fields, and the number of invasive cells was quantified using ImageJ.

Flow cytometry for detecting cell apoptosis

DSG2-knockdown NCI-H2347 cells and DSG2-overexpressing NCI-H3255 LUAD cells were used. Cells were digested with trypsin and centrifuged for 3 min at 1200×g. The cell pellet was resuspended according to the Annexin V-fluorescein isothiocyanate Apoptosis Detection Kit (C1062L; Shanghai Biyuntian Biotechnology Co., Ltd.), and apoptosis was analyzed using flow cytometry. The proportion of apoptotic cells was calculated using FlowJo, version 10.8.1.

Immunofluorescence

DSG2-knockdown NCI-H2347 cells and DSG2-overexpressing NCI-H3255 LUAD cells were used. Cells (1×10^5) were seeded into confocal-specific culture dishes (FCFC020; Shanghai Biyuntian Biotechnology Co., Ltd.) and incubated overnight. After aspirating the medium, tissue and cell fixatives were added, and the mixture was incubated at 25°C for 15 min. Cells were permeabilized with 0.1% Triton X-100 for 10 min, blocked for 1 h at 25°C with 1% bovine serum albumin/PBS, and incubated overnight at 4°C with primary antibodies. NCI-H2347 cells were incubated with Alexa Fluor® 488 secondary antibody for 1 h at room temperature in the dark, whereas NCI-H3255 cells were incubated with Alexa Fluor® 594 secondary antibody. Nuclei were stained with 1 μg/mL 4',6-diamidino-2-phenylindole (C1002; Shanghai Biyuntian Biotechnology Co., Ltd.) for 5 min. Images were captured using a confocal microscope (JEM-1400FLASH; JEOL, Ltd.), and the relative fluorescence intensity of DSG2 was calculated using ImageJ, version 1.5.2a. Antibody information and dilution ratios are listed in Supplementary Table 2.

Real-time fluorescence quantitative PCR (RT-qPCR)

(DSG2)-knockdown NCI-H2347 cells and DSG2-overexpressing NCI-H3255 LUAD cells were used. The cells were washed twice with PBS and digested with trypsin for 5 min at 37°C. Complete medium containing 10% FBS was added after detachment, and the cell suspension was centrifuged at 1200×g for 3 min. Total RNA was extracted using the TRIzol reagent (R0011; Shanghai Biyuntian Biotechnology Co., Ltd.). RNA concentration and purity were measured, and 1 μg of RNA was reverse-transcribed into complementary DNA (cDNA) using a reverse-transcription kit (D7168L; Shanghai Biyuntian Biotechnology Co., Ltd.). RT-qPCR was performed using SYBR Green qPCR Master

Mix (D7260; Shanghai Biyuntian Biotechnology Co., Ltd.). Each 10 μL reaction contained 5 μL of 2× SYBR Mix, 1 μL of cDNA template, and 0.5 μL each of forward and reverse primers (10 μmol/L). The cycling conditions were pre-denaturation at 95°C for 10 min, followed by 40 cycles of 95°C for 15 s and 60°C for 30 s. Relative mRNA expression levels were calculated using the $2^{-\Delta\Delta Ct}$ method, with glyceraldehyde-3-phosphate dehydrogenase (GAPDH) as the internal reference gene [23]. Primer sequences for RT-qPCR are listed in Supplementary Table 2.

Western blot

DSG2-knockdown NCI-H2347 cells and DSG2-overexpressing NCI-H3255 LUAD cells were used. The cell was digested with trypsin and centrifuged at 1200×g for 3 min. Cell lysis buffer (P0013; Shanghai Biyuntian Biotechnology Co., Ltd.) was added, and the lysates were incubated on ice for 30 min. Protein concentrations were measured using a bicinchoninic acid protein quantification kit (P0010S; Shanghai Biyuntian Biotechnology Co., Ltd.). Protein loading buffer (P0015L; Shanghai Biyuntian Biotechnology Co., Ltd.) was added to adjust concentrations, and samples were denatured at 95°C for 15 min. A total of 30 μg of protein per well was loaded and separated by sodium dodecyl sulfate-polyacrylamide gel electrophoresis at 120 V for 90 min. Proteins were then transferred onto a polyvinylidene difluoride (PVDF) membrane (FFP20; Shanghai Biyuntian Biotechnology Co., Ltd.) at 260 mA for 60 min. Membranes were blocked with 5% skim milk in Tris-buffered saline with 0.1% Tween-20 (TBST; ST673; Shanghai Biyuntian Biotechnology Co., Ltd.) for 2 h, followed by overnight incubation at 4°C with the corresponding primary antibody. After washing three times with TBST, membranes were incubated with secondary antibody for 2 h. Protein signals were detected using a chemiluminescent hypersensitive solution (P0018FS; Shanghai Biyuntian Biotechnology Co., Ltd.) for 10 s, and images were captured using a gel imaging system (SCG-W5000; Wuhan ServiceBio Technology Co., Ltd.). ImageJ software (version 1.5.2a) was used to quantify band intensity. Relative protein expression was calculated as the ratio of the target protein to GAPDH [24]. Antibody details and dilution ratios are listed in Supplementary Table 2.

Statistical analysis

All data were analyzed using GraphPad Prism (version 9.5.0). Each experiment included at least three distinct biological replicates ($n \geq 3$), and quantitative results are reported as mean ± standard deviation. Data normality was assessed using the Shapiro-Wilk test. For normally distributed data with equal variances (verified by Bartlett's test), comparisons between two groups were performed with an unpaired t-test; a Welch-corrected t-test was applied if the variances were heterogeneous. A one-way analysis of variance was used for comparisons among multiple groups (three or more groups of data), and additional post hoc multiple comparisons were performed if the overall difference was significant ($P < 0.05$). Tukey's method was used when the variances were homogeneous. When variances were heterogeneous, the Games-Howell test was used. For non-normally distributed data, the Kruskal-Wallis test with Dunn's post hoc test was used for multiple-group comparisons, and the Mann-Whitney U test was used for two-group comparisons. Statistical significance was defined as $P < 0.05$.

Results

Prognostic value, differential expression, and weighted gene co-expression network analysis of DSG2 in lung adenocarcinoma

Figure 1A shows that DSG2 was significantly overexpressed in LUAD. **Figure 1B** shows that patients with high DSG2 expression had a poor prognosis. To further validate the prognostic value of DSG2, we performed a survival analysis using the independent dataset GSE68465, which includes gene expression and clinical survival data from 442 LUAD samples. High DSG2 expression was significantly associated with poor patient prognosis (**Figure 1C**), and the difference in DSG2 levels between the high- and low-expression groups was statistically significant (**Figure 1D**). To systematically identify co-expression gene networks associated with DSG2 function, we conducted a weighted gene co-expression network analysis (WGCNA) using The Cancer Genome Atlas (TCGA)-LUAD dataset. We examined the scale-free topology fit index and mean connectivity under soft-thresholding powers (β) from 1 to 30 using the pick-

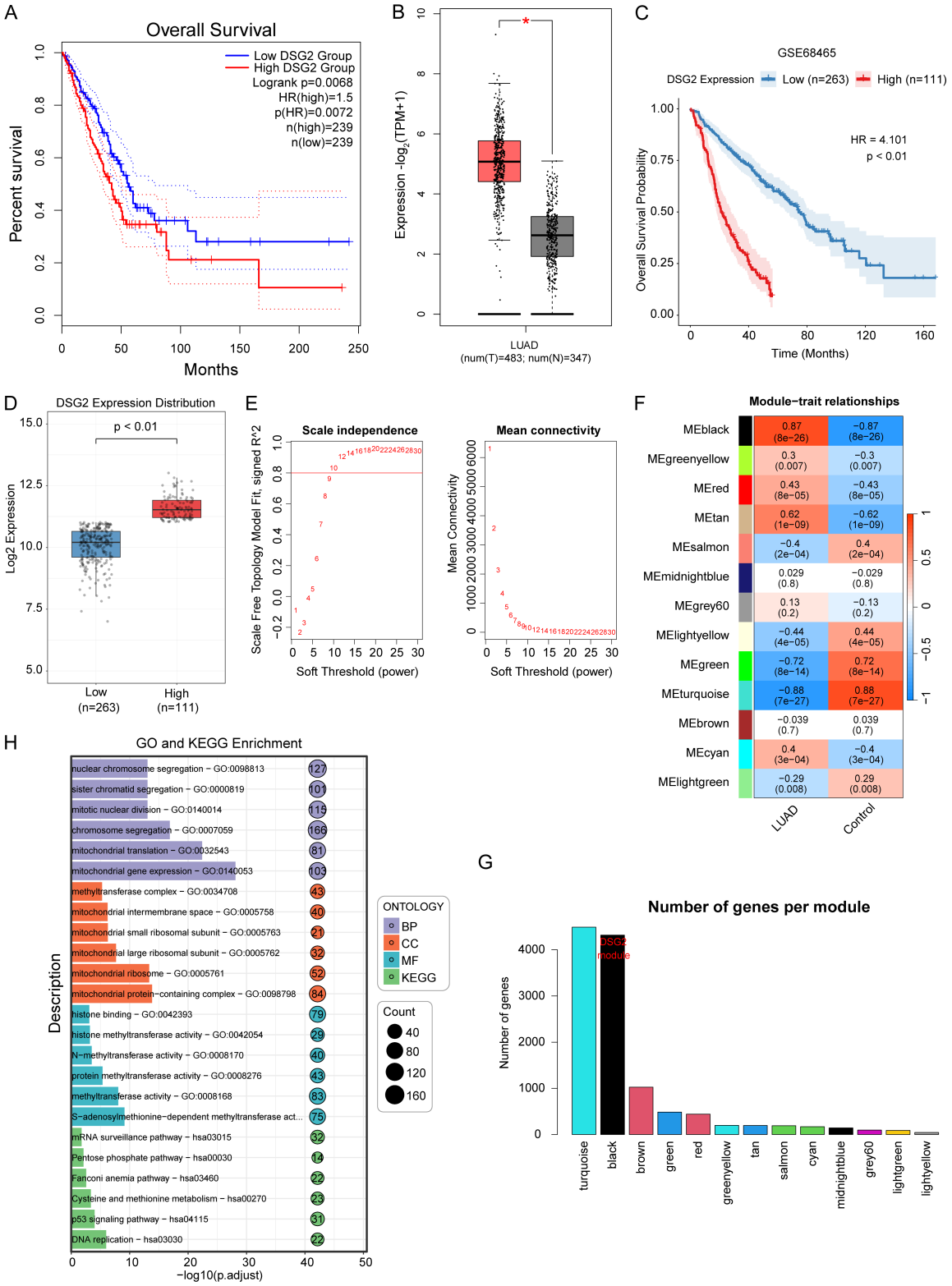

Figure 1. Prognostic value, differential expression, and weighted gene co-expression network analysis of DSG2 in lung adenocarcinoma. A. Analysis of the overall survival curves of high and low DSG2 expression in the ATGC-lung adenocarcinoma (LUAD) cohort. B. Analysis of the differential expression of DSG2 in cancerous and normal tissues in the ATGC-LUAD cohort. C. To verify the prognostic significance of DSG2 in LUAD, we conducted a survival analysis using the independent dataset GSE68465. This dataset contains gene expression and clinical survival data of 442 LUAD samples. D. Analysis of differential expression of DES2 between high-and low-expression groups in the

GSE68465 dataset. E. Scale-free topology analysis and mean connectivity analysis for each soft-thresholding power (β). F. Calculate the Pearson correlation between module eigengenes (MEs) and clinical traits (LUAD/Control) and evaluate their significance. G. The DSG2 gene was mapped to a specific module (the BLACK module). H. Genes extracted from the BLACK module for GO and KEGG functional enrichment analysis.

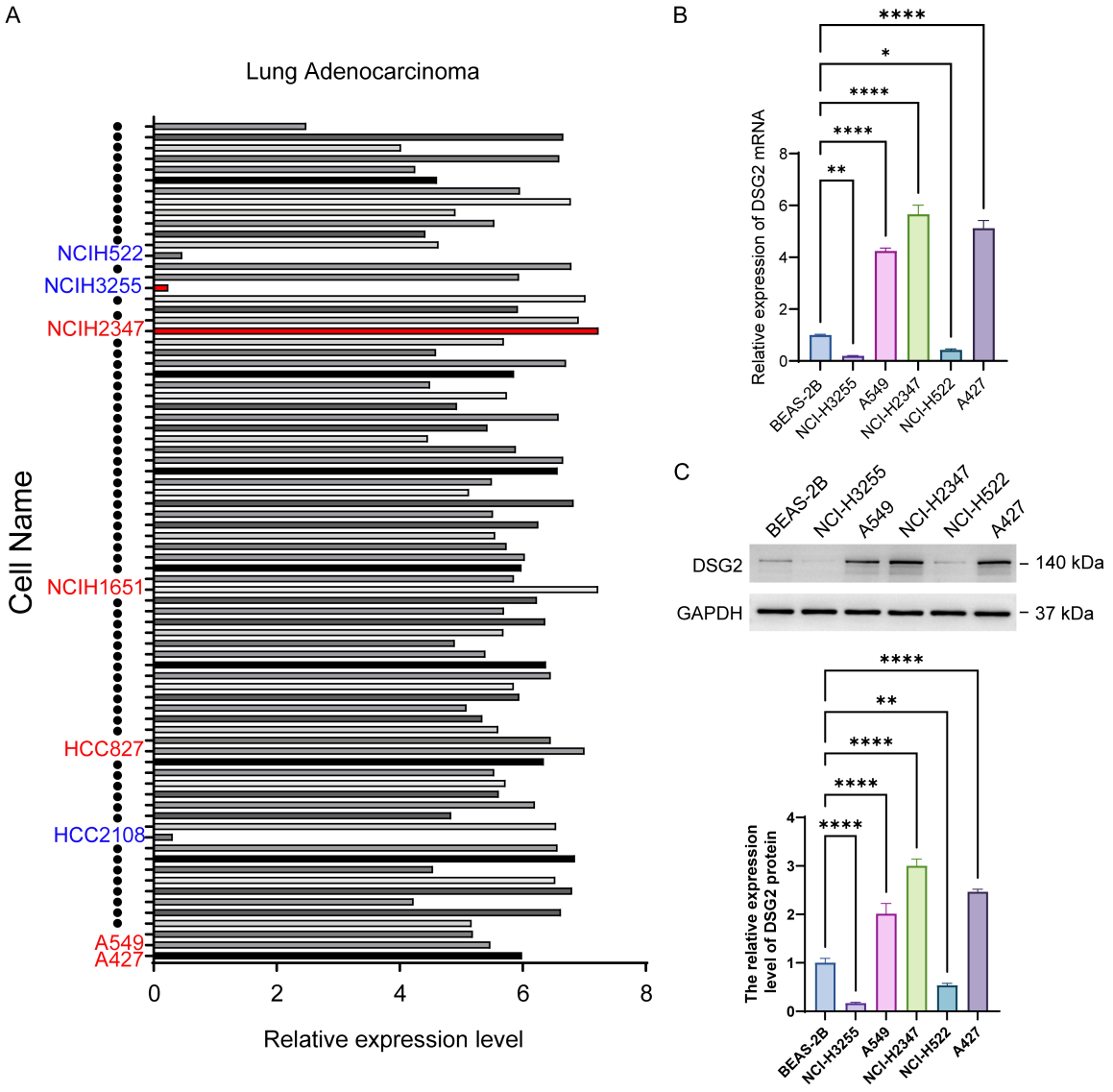

Figure 2. High expression of DSG2 in lung adenocarcinoma tissues and cells. A. Analysis of the differential expression of DSG2 in different lung adenocarcinoma cells using the CCEL database (red marks represent cell lines with significantly high expression, and blue marks represent cell lines with significantly low expression). B. RT-qPCR was used to detect the relative expression levels of DSG2 mRNA in lung adenocarcinoma cells NCI-H3255, NCI-H2347, NCI-H522, A549, A427, and normal lung epithelial cells BEAS-2B. C. Western blot was used to detect the relative expression levels of DSG2 protein in lung adenocarcinoma cells NCI-H3255, NCI-H2347, NCI-H522, A549, A427, and normal lung epithelial cells BEAS-2B. *$P < 0.05$, **$P < 0.01$, ****$P < 0.0001$.

SoftThreshold function. We selected the lowest power that achieved a scale-free topology fit index (R^2) ≥ 0.8 as the soft threshold, at which point the network met scale-free distribution characteristics while maintaining appropriate sparsity (**Figure 1E**). Subsequently, we calculated the Pearson correlation between module eigengenes (MEs) and clinical traits (LUAD vs. Control). The Black module exhibited the strongest positive correlation with LUAD status

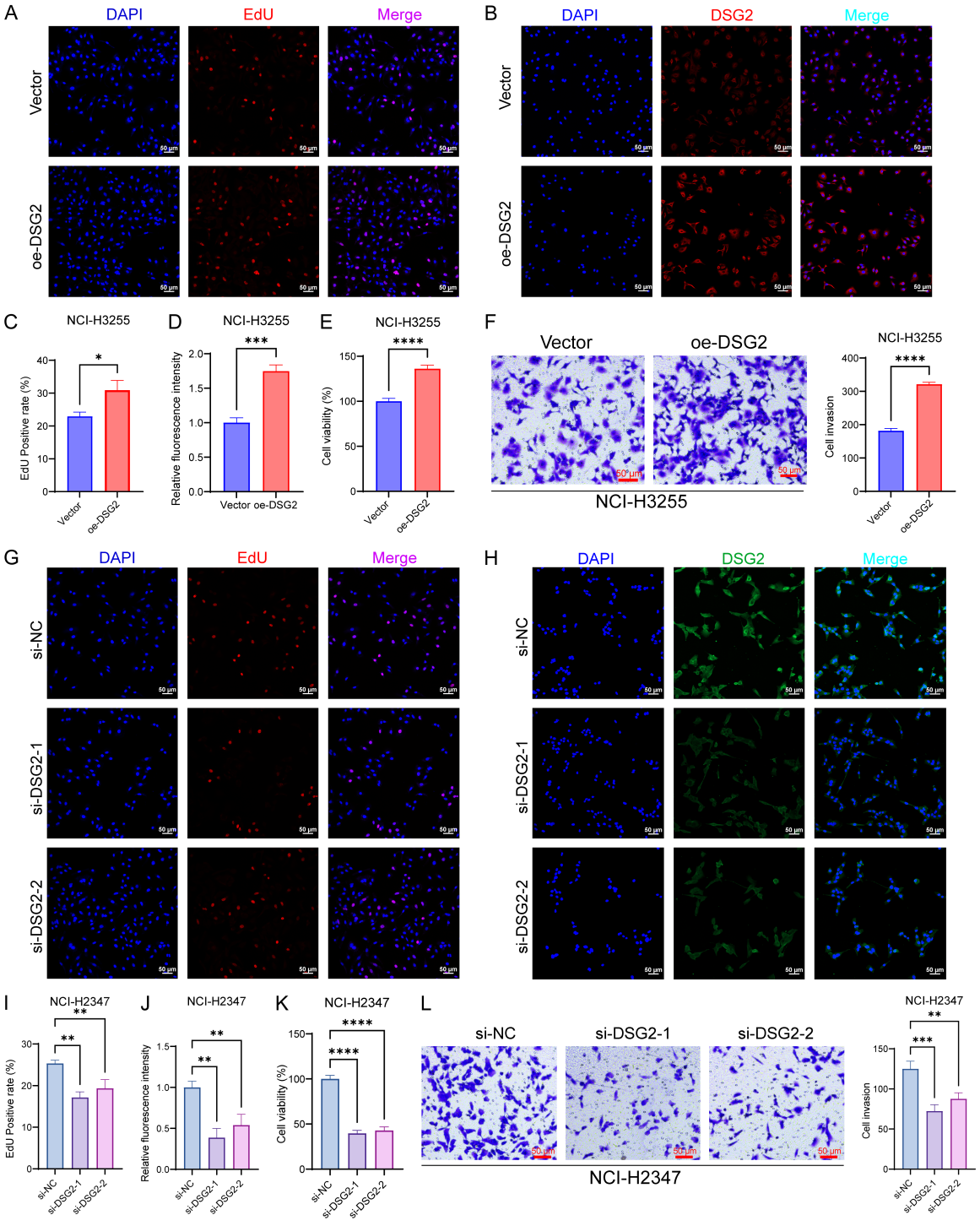

Figure 3. DSG2 induces proliferation and invasion of lung adenocarcinoma cells. A. After constructing a DSG2 overexpressing cell line in NCI-H3255 cells for 48 h, the change in cell proliferation ability was detected by the EDU assay (×200, scale bar: 50 μm). B. The expression level of DSG2 was detected by immunofluorescence assay in NCI-H3255 cells overexpressing DSG2 (×200, scale bar: 50 μm). C. Bar chart of the statistical analysis of the EDU assay in NCI-H3255 cells. D. Bar chart of the statistical analysis of immunofluorescence in NCI-H3255 cells. E. The change in cell proliferation ability was detected by the CCK8 assay in NCI-H3255 cells overexpressing DSG2. F. The change in cell invasion ability was detected using the Transwell assay in NCI-H3255 cells overexpressing DSG2 (×200, scale bar: 50 μm). G. After constructing a DSG2-knockdown cell line in NCI-H2347 cells for 48 h, the change in cell proliferation ability was detected by the EDU assay (×200, scale bar: 50 μm). H. The expression level of DSG2 was detected by immunofluorescence assay in NCI-H2347 cells with DSG2 knockdown (×200, scale bar: 50 μm). I. Bar chart of the statistical analysis of the EDU assay in NCI-H2347 cells. J. Bar chart of the statistical analysis of

immunofluorescence in NCI-H2347 cells. K. The change in cell proliferation ability was detected by the CCK8 assay in NCI-H2347 cells with DSG2 knockdown. L. The change in cell invasion ability was detected by the Transwell assay in NCI-H2347 cells with DSG2 knockdown (×200, scale bar: 50 μm). *P < 0.05, **P < 0.01, ***P < 0.001, ****P < 0.0001.

(**Figure 1F**), and DSG2 was significantly enriched in this module (**Figure 1G**). Functional enrichment analysis of genes in the Black module showed that Gene Ontology (GO) and Kyoto Encyclopedia of Genes and Genomes (KEGG) results were primarily associated with mitochondrial gene expression, mitochondrial protein-containing complexes, and deoxyribonucleic acid (DNA) replication (**Figure 1H**).

High expression of DSG2 in lung adenocarcinoma cells and tissues

Using the Cancer Cell Line Encyclopedia (CCEL) database, we analyzed the relative expression levels of DSG2 in various LUAD cell lines (**Figure 2A**) and discovered that DSG2 was highly expressed in most LUAD cells. DSG2 was significantly overexpressed in NCI-H2347, NCI-H1651, HCC827, A549, and A427 cells, whereas its expression was significantly lower in NCI-H522, NCI-H3255, and HCC2108 cells. Based on these differences, we constructed overexpression models in LUAD cell lines with low DSG2 expression and knockdown models in those with significantly high expression. We selected five LUAD cell lines with the most significant differential DSG2 expression according to the CCLE database. Western blotting and reverse transcription quantitative polymerase chain reaction (RT-qPCR) results demonstrated that NCI-H2347 cells had significantly higher DSG2 messenger ribonucleic acid (mRNA) and protein levels than NCI-H3255 cells (**Figure 2B** and **2C**). Thus, we established a DSG2 knockdown model using NCI-H2347 cells and a DSG2 overexpression model using NCI-H3255 cells. RT-qPCR confirmed the successful construction of both models (Supplementary Figure 1).

DSG2 promotes proliferation and invasion of LUAD cells and inhibits anoikis

We assessed the effects of DSG2 expression on LUAD cell invasion and proliferation using 5-ethynyl-2'-deoxyuridine (EdU), cell counting kit-8 (CCK-8), and Transwell assays. Overexpression of DSG2 significantly increased the proportion of EdU-positive cells, and DSG2 was mainly localized in the cytoplasm (**Figure 3A-D**). The CCK-8 assay showed that DSG2 overexpression improved the viability of NCI-H3255 cells (**Figure 3E**), while the Transwell assay demonstrated that overexpression also enhanced their invasive capacity (**Figure 3F**). Conversely, DSG2 knockdown in NCI-H2347 cells significantly reduced proliferation and invasion (**Figure 3G-L**).

Subsequently, we investigated how differential DSG2 expression affects anoikis in LUAD cells. Morphological changes in NCI-H2347 and NCI-H3255 cells were observed 48 h after transfection using a microscope. No significant differences were observed in cell morphology following DSG2 overexpression. However, following DSG2 knockdown, the volume of suspended cells significantly decreased, and numerous vesicular protrusions were induced on the cell surface (**Figure 4A**). Flow cytometry analysis of apoptosis indicated that DSG2 knockdown significantly increased the proportion of apoptotic cells, while DSG2 overexpression had no significant effect (**Figure 4B** and **4C**). These results suggest that DSG2 inhibits anoikis in LUAD cells.

To further validate this effect, we examined the expression of proteins associated with anoikis. DSG2 knockdown markedly decreased the levels of P53 and Bcl-2, while increasing the levels of Bcl-2-associated X protein (Bax) and the ratio of cleaved-caspase-3/caspase-3 significantly. In contrast, DSG2 overexpression produced the opposite changes in these anoikis-related proteins (**Figure 4D** and **4E**), confirming that DSG2 inhibits anoikis in LUAD cells.

DSG2 activates the integrin β1/FAK signaling pathway

To investigate how DSG2 regulates invasion, proliferation, and anoikis in LUAD cells, we examined the expression of proteins involved in the integrin β1/FAK signaling pathway by western blotting. DSG2 knockdown significantly reduced the ratios of integrin β1/phosphorylated integrin β1 (p-integrin β1) and FAK/p-FAK, suggesting suppression of the integrin β1/FAK pathway. In contrast, DSG2 overexpression sig-

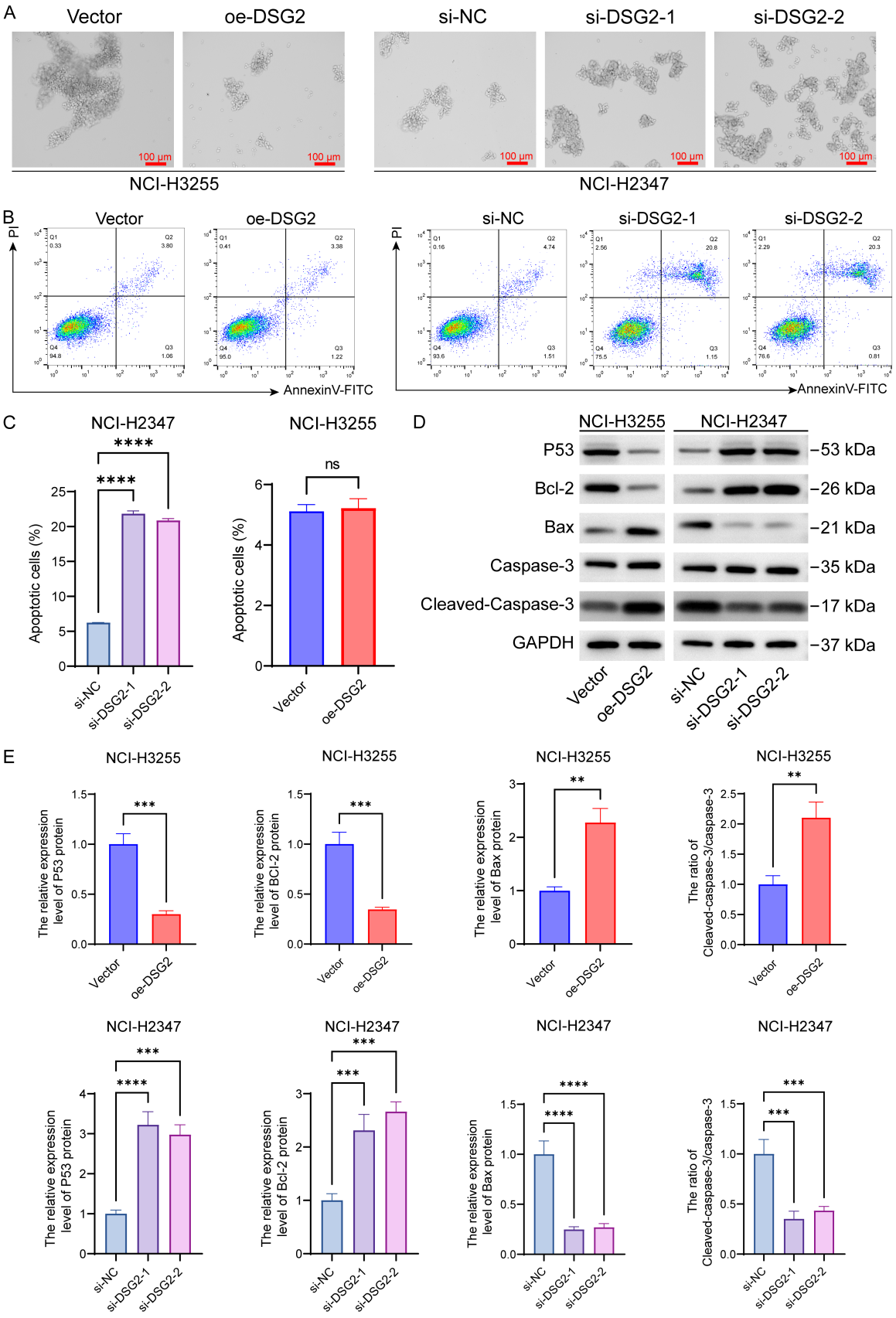
A
Vector
oe-DSG2
si-NC
si-DSG2-1
si-DSG2-2
100 μm
NCI-H3255
NCI-H2347
B
PI
AnnexinV-FITC
C
NCI-H2347
NCI-H3255
Apoptotic cells (%)
ns
D
NCI-H3255
NCI-H2347
P53
Bcl-2
Bax
Caspase-3
Cleaved-Caspase-3
GAPDH
-53 kDa
-26 kDa
-21 kDa
-35 kDa
-17 kDa
-37 kDa
E
The relative expression level of P53 protein
The relative expression level of Bcl-2 protein
The relative expression level of Bax protein
The ratio of Cleaved-caspase-3/caspase-3

Figure 4. DSG2 inhibits anoikis in lung adenocarcinoma cells. A. After transfecting the DSG2-overexpressing plasmid into NCI-H3255 cells and interfering RNA into NCI-H2347 cells for 48 h, the morphological changes of anoikis in NCI-H3255 cells and NCI-H2347 cells were observed in ultra-low attachment culture (×100, scale bar: 100 μm). B. The change in the proportion of apoptotic cells was detected by flow cytometry in NCI-H3255 cells and NCI-H2347 cells. C. Bar chart of statistical analysis of flow-cytometric detection of cell apoptosis. D. Western blot was used to detect the changes in the relative expression levels of anoikis-related proteins P53, Bcl-2, Bax, Caspase-3, and Cleaved-caspase-3 in NCI-H3255 cells and NCI-H2347 cells. E. Bar chart of statistical analysis of Western blot. *P < 0.05, **P < 0.01, ***P < 0.001, ****P < 0.0001, "ns" represents P > 0.05.

nificantly increased these ratios, activating the integrin β1/FAK signaling pathway (**Figure 5A**). We also detected changes in proteins related to the integrin β1/FAK signaling pathway. Following DSG2 knockdown, the ratios of integrin β1/p-integrin β1 and FAK/p-FAK were significantly inhibited, whereas the addition of Pyrintegrin restored the ratios of integrin β1/p-integrin β1 and FAK/p-FAK, reactivating the signaling pathway (**Figure 5B**) and confirming that DSG2 inhibits anoikis while promoting invasion and proliferation of LUAD cells. Conversely, treatment with ATN-161, an integrin β1/FAK inhibitor, further suppressed the phosphorylation of integrin β1 and FAK after DSG2 knockdown, enhancing pathway inhibition (**Figure 5C**). These complementary interventions confirm that DSG2 exerts its functional effects in LUAD cells specifically by modulating the integrin β1/FAK signaling pathway.

Pyrintegrin reverses the effects of DSG2 knockdown on LUAD cells and anoikis

To confirm that DSG2 regulates LUAD cell invasion, proliferation, and anoikis through the integrin β1/FAK signaling pathway, we treated cells with Pyrintegrin, an integrin β1 agonist, and assessed phenotypic changes. DSG2 knockdown significantly reduced the proportion of EdU-positive cells, decreased cytoplasmic DSG2 expression, and inhibited cell viability and invasion. Pyrintegrin treatment reversed these effects (**Figure 6A-F**).

After DSG2 knockdown, suspended cell volume decreased, apoptosis increased, and the expression of anoikis-related proteins p53 and Bcl-2 decreased, while Bax and the ratio of cleaved-caspase-3/caspase-3 significantly increased. Furthermore, Pyrintegrin restored these protein levels and reversed the increase in anoikis induced by DSG2 knockdown (**Figure 6C-I**). These results confirm that DSG2 suppresses anoikis and promotes LUAD cell proliferation and invasion via the integrin β1/FAK pathway.

ATN-161 reverses the promotive effects of DSG2 overexpression on LUAD cells and induces anoikis

To further confirm that DSG2 promotes LUAD cell proliferation and invasion while inhibiting anoikis through the integrin β1/FAK signaling pathway, we treated cells with ATN-161, an integrin β1 antagonist, and evaluated phenotypic changes. DSG2 overexpression significantly increased the proportion of EdU-positive cells, enhanced cytoplasmic DSG2 expression, and promoted cell viability and invasion. ATN-161 treatment effectively counteracted these effects (**Figure 7A-F**). Morphologically, DSG2 overexpression prevented the cell shrinkage typically associated with anoikis and reduced apoptosis. At the molecular level, DSG2 overexpression downregulated the levels of pro-anoikis proteins p53 and Bax, upregulated the anti-apoptotic protein Bcl-2, and decreased the cleaved-caspase-3/caspase-3 ratio. ATN-161 reversed these regulatory changes, restoring anoikis morphology and the expression of related proteins (**Figure 7G-I**).

Discussion

In this study, we investigated the role and mechanism of DSG2 in LUAD. DSG2 was highly expressed in LUAD cells and tissues, and elevated DSG2 levels were associated with poor prognosis. Using DSG2 overexpression and knockdown models in different LUAD cell lines, we discovered that DSG2 overexpression significantly enhanced proliferation and invasion while inhibiting anoikis, whereas DSG2 knockdown produced the opposite effects. These findings suggest that DSG2 is essential for tumor growth, progression, and metastasis in LUAD and may serve as a valuable molecular marker for prognosis and therapeutic strategy development. Previous studies have shown that under anoikis stress, p53 accumulates and becomes activated. As a transcription factor, p53 increases the transcription of the anti-apoptotic protein Bcl-2 and upregulates the

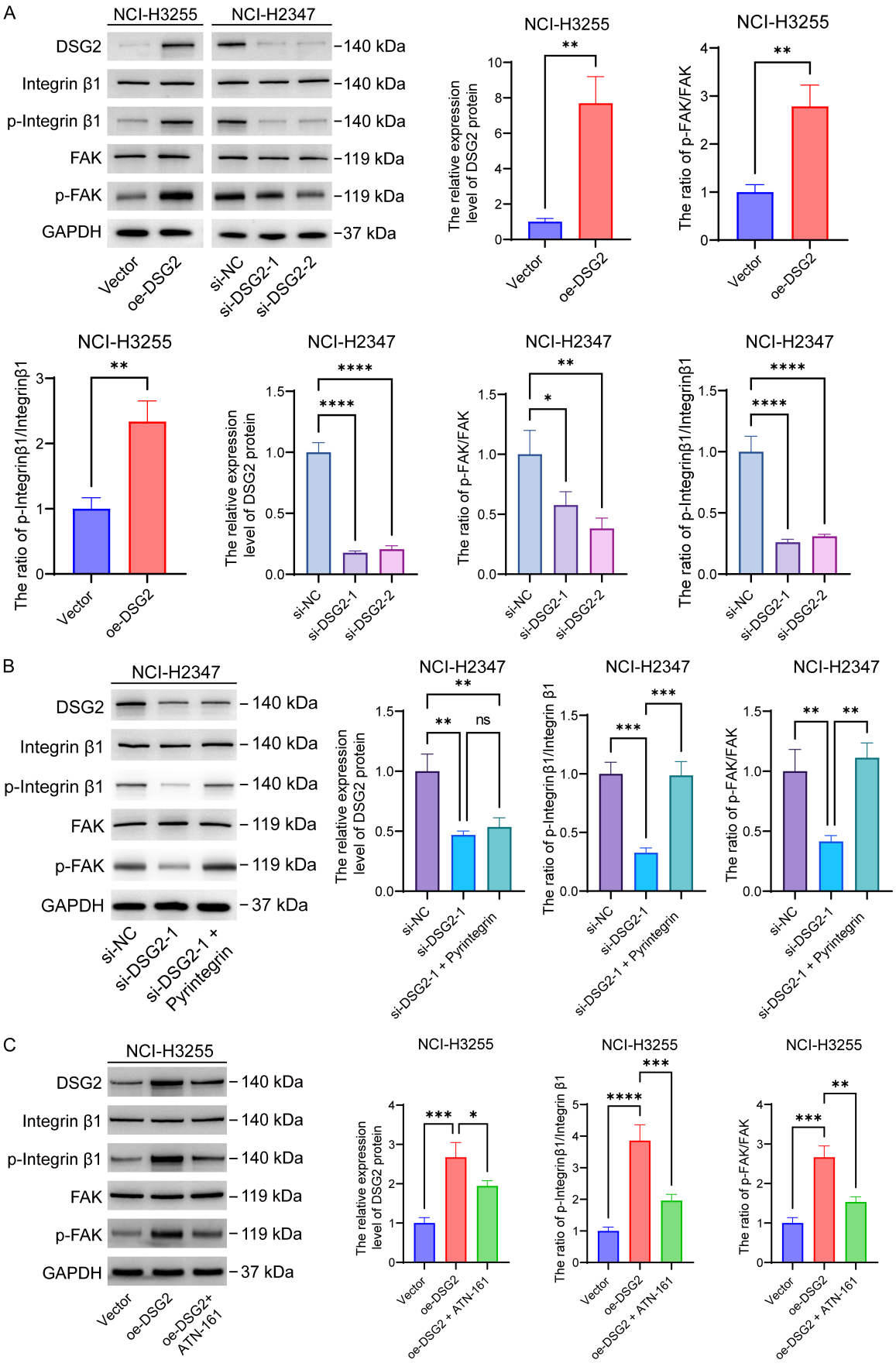
A
NCI-H3255
NCI-H2347
DSG2
Integrin β1
p-Integrin β1
FAK
p-FAK
GAPDH
140 kDa
140 kDa
140 kDa
119 kDa
119 kDa
37 kDa
Vector
oe-DSG2
si-NC
si-DSG2-1
si-DSG2-2
The relative expression level of DSG2 protein
The ratio of p-FAK/FAK
The ratio of p-Integrinβ1/Integrinβ1
B
si-DSG2-1 + Pyrintegrin
C
oe-DSG2+ ATN-161
oe-DSG2 + ATN-161

Figure 5. DSG2 activates the integrin β1/FAK signaling pathway. A. After transfecting the DSG2-overexpressing plasmid into NCI-H3255 cells and interfering RNA into NCI-H2347 cells for 48 h, a Western blot was used to detect the changes in the relative expression levels of proteins related to the integrin β1/FAK signaling pathway, including integrin β1, p-integrin β1, FAK, p-FAK, and DSG2 in NCI-H3255 cells and NCI-H2347 cells. B. After constructing a DSG2-knockdown cell line in NCI-H2347 cells, Pyrintegrin was added, and incubation continued for 24 h. Western blot was used to detect the changes in the relative expression levels of proteins related to the integrin β1/FAK signaling pathway, including integrin β1, p-integrin β1, FAK, p-FAK, and DSG2 in NCI-H2347 cells. C. After successfully establishing a DSG2-knockdown cell line in NCI-H2347 cells, ATN-161 (an inhibitor of the integrin β1/FAK signaling pathway) was added. Subsequently, the expression levels of proteins, including integrin β1, p-integrin β1, FAK, p-FAK, and DSG2, were detected through Western blot experiments. $^{*}P < 0.05$, $^{**}P < 0.01$, $^{***}P < 0.001$, $^{****}P < 0.0001$, "ns" represents $P > 0.05$.

pro-apoptotic protein Bax, disrupting the Bcl-2/Bax balance and triggering apoptosis [25]. Bcl-2, located on the mitochondrial membrane, inhibits apoptosis by preserving membrane integrity and inhibiting cytochrome c release.

Caspases are activated by mitochondrial cytochrome c. Caspase-3 is an effector protease that is cleaved into its active form, cleaved-caspase-3, which hydrolyzes cellular structural proteins, including cytoskeletal and nuclear lamin proteins, directly causing typical anoikis morphological changes such as cell shrinkage, membrane blebbing, and apoptotic body formation [26-28]. In this study, DSG2 knockdown induced anoikis in LUAD cells by increasing the levels of Bax and the ratio of cleaved-caspase-3/caspase-3 while decreasing p53 and Bcl-2 levels. Previous studies reported that DSG2-related apoptosis is mediated by caspase-3 [29] and involves the p53 pathway, consistent with our findings [30].

The integrin β1/FAK signaling pathway is a classical anoikis-related pathway [31, 32]. Integrin β1, a major transmembrane receptor, initiates focal adhesion assembly by recognizing ECM components such as fibronectin [32, 33], activating FAK autophosphorylation. Phosphorylated FAK recruits downstream signaling molecules to maintain cell viability during matrix detachment. When cells detach from the ECM [34], integrin β1/FAK signaling is inactivated, leading to upregulation of pro-apoptotic proteins such as Bax, release of mitochondrial cytochrome c, activation of caspase-3, and apoptosis [35, 36]. Previous studies have confirmed that DSG2 regulates FAK in cell migration, adhesion, and angiogenesis [37, 38]; however, its role in the integrin β1/FAK signaling pathway remain unexplored. According to our mechanistic research, DSG2 activates the integrin β1/FAK signaling pathway, thereby regulating multiple processes, including cell adhesion, invasion, proliferation, and survival. In this study, DSG2 overexpression significantly increased FAK and integrin β1 phosphorylation, thereby activating the integrin β1/FAK signaling pathway and enhancing LUAD cell proliferation, invasion, and anoikis resistance. Conversely, DSG2 knockdown inhibited this pathway, revealing part of the molecular mechanism by which DSG2 functions in LUAD and providing a theoretical foundation for targeting this signaling pathway therapeutically. Furthermore, treatment with the integrin β1 agonist Pyrintegrin reversed the effects of DSG2 knockdown on LUAD cell proliferation, invasion, and anoikis, confirming that DSG2 operates via this signaling pathway. These findings suggest that controlling the integrin β1/FAK signaling pathway may be a novel therapeutic strategy for LUAD. Our study proposes a novel mechanism in which DSG2 activates the integrin β1/FAK signaling pathway, while DSG2 knockdown inhibits proliferation and invasion and induces anoikis in LUAD cells.

This study has certain limitations. First, the research mainly focused on cellular models and lacked validation in vivo experiments. Cellular experiments provide direct evidence; however, in vivo environments are more complex, and the effects of DSG2 on LUAD biological behavior and associated signaling pathways may be influenced by multiple factors. The current rescue experiments do not have control groups with 'pathway modulator treatment alone'. Although the existing experimental logic of 'genetic intervention-pharmacological reversal' and the known specificities of the tool compounds strongly support the conclusion that DSG2 acts through the integrin β1/FAK pathway, future research still needs to set up more comprehensive control groups to completely rule out potential non-specific effects of the

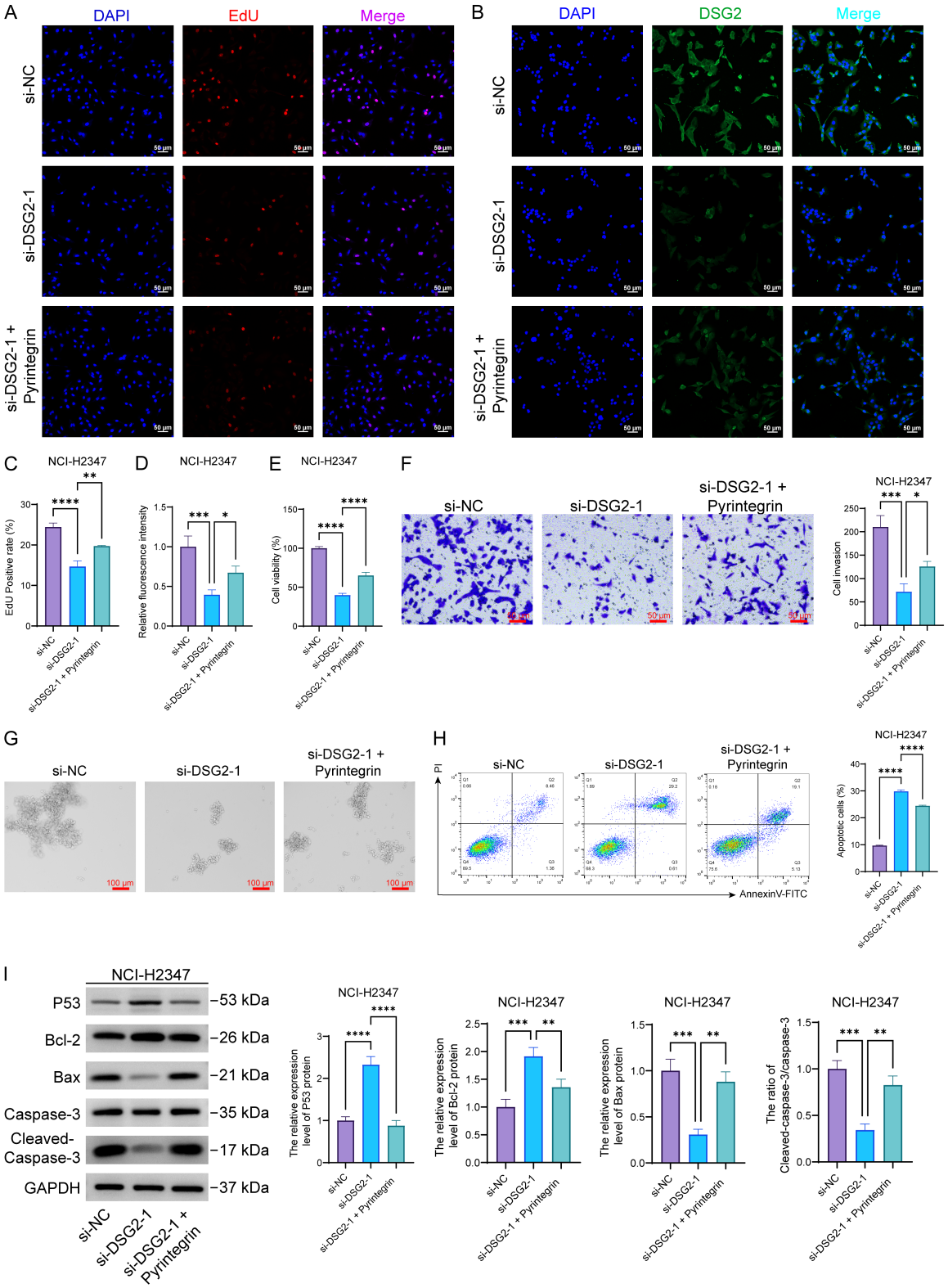

Figure 6. Pyrintegrin counteracts the inhibitory effects of DSG2 knockdown on the NCI-H2347 Cells, as well as its promoting effect on anoikis. A. After constructing a DSG2-knockdown cell line in NCI-H2347 cells, Pyrintegrin was added, and incubation continued for 24 h. The change in cell proliferation ability was detected using the EDU assay (×200, scale bar: 50 μm). B. The expression level of DSG2 was detected by immunofluorescence assay in NCI-H2347 cells (×200, scale bar: 50 μm). C. Bar chart of the statistical analysis of the experiment in NCI-H2347 cells.

D. Bar chart of the statistical analysis of immunofluorescence in NCI-H2347 cells. E. The change in cell proliferation ability was detected by the CCK8 assay in NCI-H2347 cells. F. The change in cell invasion ability was detected using the Transwell assay in NCI-H2347 cells (×200, scale bar: 50 μm). G. The morphological changes of anoikis in NCI-H3255 cells and NCI-H2347 cells were observed in NCI-H2347 cells (×100, scale bar: 100 μm). H. The change in the proportion of apoptotic cells was detected by flow cytometry in NCI-H2347 cells. I. Western blot was used to detect the changes in the relative expression levels of anoikis-related proteins P53, Bcl-2, Bax, Caspase-3, and Cleaved-caspase-3 in NCI-H2347 cells. *$P < 0.05$, **$P < 0.01$, ***$P < 0.001$, ****$P < 0.0001$.

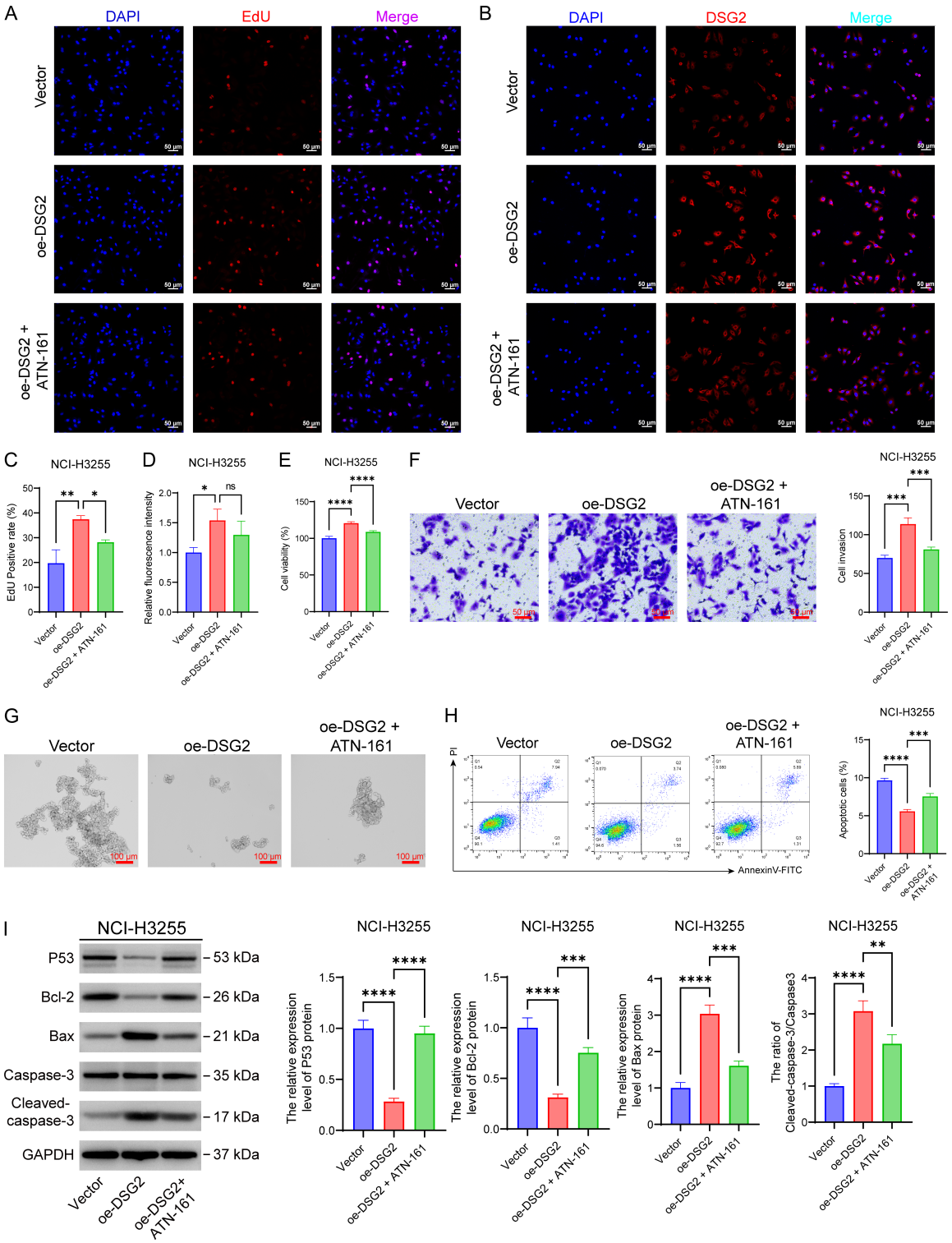

Figure 7. ATN-161 counteracts the promotive effects of DSG2 overexpression on proliferation and invasion in NCI-H3255 cells and induces anoikis. A. After establishing the DSG2-overexpressing cell line in NCI-H3255 cells, ATN-161 was added, and incubation continued for 24 hours. Changes in cell proliferation capacity were detected using the EdU assay (×200, scale bar: 50 μm). B. The expression level of DSG2 in NCI-H3255 cells was detected by immunofluorescence (×200, scale bar: 50 μm). C. Statistical analysis bar chart for the NCI-H3255 cell experiment. D. Statistical analysis bar chart for NCI-H3255 cell immunofluorescence. E. Changes in the proliferation capacity of NCI-H3255 cells were detected by the CCK-8 assay. F. Changes in the invasive capacity of NCI-H3255 cells were detected by the Transwell assay (×200, scale bar: 50 μm). G. Morphological changes of anoikis were observed in NCI-H3255 cells (×100, scale bar: 100 μm). H. Changes in the proportion of apoptotic NCI-H3255 cells were detected by flow cytometry. I. Changes in the relative expression levels of anoikis-related proteins P53, Bcl-2, Bax, Caspase-3, and Cleaved-caspase-3 in NCI-H3255 cells were detected by Western blot. $*P < 0.05$, $**P < 0.01$, $***P < 0.001$, $****P < 0.0001$, "ns" represents $P > 0.05$.

modulators and further confirm the accuracy of this mechanism. Future studies using animal models are required to comprehensively elucidate the role and mechanism of DSG2. Second, we examined only the integrin β1/FAK signaling pathway. DSG2 may also act through other signaling pathways or molecular mechanisms, necessitating further investigation of its downstream network. Third, while we explored the association between DSG2 expression and prognosis using online databases, the limited sample size and lack of direct validation in clinical samples require confirmation through large-scale clinical studies. Future work should systematically collect LUAD and paired adjacent tissues to validate DSG2 expression and its co-localization with p-FAK, enhancing the translational significance of this study. Furthermore, integrating public single-cell datasets or performing independent sequencing could clarify DSG2 expression patterns across cell subtypes, including malignant epithelial cells, tumor-infiltrating immune cells (such as T cells and macrophages), and cancer-associated fibroblasts.

Conclusion

DSG2 is highly expressed in LUAD tissues and cells and is associated with poor prognosis. DSG2 overexpression suppresses anoikis and promotes LUAD cell invasion and proliferation. These effects are mediated through activation of the integrin β1/FAK signaling pathway, and treatment with Pyrintegrin reverses the effects of DSG2 knockdown on LUAD cells. Thus, DSG2 is a potential therapeutic target for LUAD and provides a theoretical basis for targeted therapy. Further studies are required to validate its role in in vivo models and to investigate its downstream signaling network to fully understand the functions and mechanisms of DSG2 in LUAD.

Disclosure of conflict of interest

None.

Address correspondence to: Zhigang Cai, The First Department of Pulmonary and Critical Care Medicine, The Second Hospital of Hebei Medical University, 215 Heping West Road, Shijiazhuang 050000, Hebei, China. Tel: +86-18233106552; E-mail: zhigang_cai@hebmu.edu.cn

References

[1] Kim N, Kim HK, Lee K, Hong Y, Cho JH, Choi JW, Lee JI, Suh YL, Ku BM, Eum HH, Choi S, Choi YL, Joung JG, Park WY, Jung HA, Sun JM, Lee SH, Ahn JS, Park K, Ahn MJ and Lee HO. Single-cell RNA sequencing demonstrates the molecular and cellular reprogramming of metastatic lung adenocarcinoma. Nat Commun 2020; 11: 2285.

[2] Hutchinson BD, Shroff GS, Truong MT and Ko JP. Spectrum of lung adenocarcinoma. Semin Ultrasound CT MR 2019; 40: 255-264.

[3] Denisenko TV, Budkevich IN and Zhivotovsky B. Cell death-based treatment of lung adenocarcinoma. Cell Death Dis 2018; 9: 117.

[4] Mo G, Long X, Hu Z, Tang Y and Zhou Z. Anoikis-related gene signatures can aid prognosis of lung adenocarcinoma. Adv Clin Exp Med 2024; 33: 751-761.

[5] Qin H, Wang Q, Xu J, Zeng H, Liu J, Yu F and Yang J. Integrative analysis of anoikis-related genes prognostic signature with immunotherapy and identification of CDKN3 as a key oncogene in lung adenocarcinoma. Int Immunopharmacol 2024; 143: 113282.

[6] Taddei ML, Giannoni E, Fiaschi T and Chiarugi P. Anoikis: an emerging hallmark in health and diseases. J Pathol 2012; 226: 380-393.

[7] Wang Y, Cheng S, Fleishman JS, Chen J, Tang H, Chen ZS, Chen W and Ding M. Targeting anoikis resistance as a strategy for cancer therapy. Drug Resist Updat 2024; 75: 101099.

[8] Han YH, Wang Y, Lee SJ, Jin MH, Sun HN and Kwon T. Regulation of anoikis by extrinsic

death receptor pathways. Cell Commun Signal 2023; 21: 227.
[9] Kim EY, Cha YJ, Jeong S and Chang YS. Overexpression of CEACAM6 activates Src-FAK signaling and inhibits anoikis, through homophilic interactions in lung adenocarcinomas. Transl Oncol 2022; 20: 101402.
[10] Wang C, Wang T, Lv D, Li L, Yue J, Chen HZ and Xu L. Acquired resistance to EGFR TKIs mediated by TGFβ1/Integrin β3 signaling in EGFR-mutant lung cancer. Mol Cancer Ther 2019; 18: 2357-2367.
[11] Wu JI, Lin YP, Tseng CW, Chen HJ and Wang LH. Crabp2 promotes metastasis of lung cancer cells via HuR and integrin β1/FAK/ERK signaling. Sci Rep 2019; 9: 845.
[12] Corbet C, Bastien E, Santiago de Jesus JP, Dierge E, Martherus R, Vander Linden C, Doix B, Degavre C, Guilbaud C, Petit L, Michiels C, Dessy C, Larondelle Y and Feron O. TGFβ2-induced formation of lipid droplets supports acidosis-driven EMT and the metastatic spreading of cancer cells. Nat Commun 2020; 11: 454.
[13] Dong B, Gu Y, Sun X, Wang X, Zhou Y, Rong Z, Zhang J, Shi X, Zhang Z, He X, Chen L, Xiong Q, Pang X and Cui Y. Targeting TUBB3 suppresses anoikis resistance and bone metastasis in prostate cancer. Adv Healthc Mater 2024; 13: e2400673.
[14] Ungewiß H, Rötzer V, Meir M, Fey C, Diefenbacher M, Schlegel N and Waschke J. Dsg2 via Src-mediated transactivation shapes EGFR signaling towards cell adhesion. Cell Mol Life Sci 2018; 75: 4251-4268.
[15] Lee K, Lee SH, Kim W, Lee J, Park JG, Kim JS, Kim JT, Kang YE, Shong M, Lee HJ, Kim JM, Kim WG, Koo BS, Kim KS and Min JK. Dsg2-mediated c-Met activation in anaplastic thyroid cancer motility and invasion. Endocr Relat Cancer 2020; 27: 601-614.
[16] Myo Min KK, Ffrench CB, McClure BJ, Ortiz M, Dorward EL, Samuel MS, Ebert LM, Mahoney MG and Bonder CS. Desmoglein-2 as a cancer modulator: friend or foe? Front Oncol 2023; 13: 1327478.
[17] Wang L, Lv Y, Li J, Nan Y, Piao L and Liang Z. Downregulation of desmoglein 2 promotes EMT progression in gallbladder cancer. Histol Histopathol 2023; 38: 467-474.
[18] Yang T, Jia L, Bian S, Chang X, Zhang Q, Tang Q, Zhu J, Yang Z and Feng Z. TROP2 down-regulated DSG2 to promote gastric cancer cell invasion and migration by EGFR/AKT and DSG2/PG/β-catenin pathways. Curr Cancer Drug Targets 2022; 22: 691-702.
[19] Wang CC, Lin JY, Wang CY, Shen WJ, Liao PC, Ho YF, Lin CW, Wang SA, Ko CC, Dey S, Ta HDK, Xuan DTM, Kumar S, William BT, Wang JM and Wang WJ. DSG2 attenuates gemcitabine efficacy through PTX3 in lung adenocarcinoma. Biochim Biophys Acta Mol Basis Dis 2025; 1871: 167881.
[20] Su C, Liu WX, Wu LS, Dong TJ and Liu JF. Screening of hub gene targets for lung cancer via microarray data. Comb Chem High Throughput Screen 2021; 24: 269-285.
[21] Ranstam J and Cook JA. Kaplan-meier curve. Br J Surg 2017; 104: 442.
[22] Lee HW, Khan SQ, Faridi MH, Wei C, Tardi NJ, Altintas MM, Elshabrawy HA, Mangos S, Quick KL, Sever S, Reiser J and Gupta V. A podocyte-based automated screening assay identifies protective small molecules. J Am Soc Nephrol 2015; 26: 2741-2752.
[23] Bong D, Sohn J and Lee SV. Brief guide to RT-qPCR. Mol Cells 2024; 47: 100141.
[24] Pillai-Kastoori L, Schutz-Geschwender AR and Harford JA. A systematic approach to quantitative western blot analysis. Anal Biochem 2020; 593: 113608.
[25] Babaei G, Aliarab A, Asghari Vostakolaei M, Hotelchi M, Neisari R, Gholizadeh-Ghaleh Aziz S and Bazl MR. Crosslink between p53 and metastasis: focus on epithelial-mesenchymal transition, cancer stem cell, angiogenesis, autophagy, and anoikis. Mol Biol Rep 2021; 48: 7545-7557.
[26] Lin D, Feng J and Chen W. Bcl-2 and caspase-8 related anoikis resistance in human osteosarcoma MG-63 cells. Cell Biol Int 2008; 32: 1199-1206.
[27] Yang SD, Bai ZL, Zhang F, Ma L, Yang DL and Ding WY. Levofloxacin increases the effect of serum deprivation on anoikis of rat nucleus pulposus cells via Bax/Bcl-2/caspase-3 pathway. Toxicol Mech Methods 2014; 24: 688-696.
[28] Hausmann M, Leucht K, Ploner C, Kiessling S, Villunger A, Becker H, Hofmann C, Falk W, Krebs M, Kellermeier S, Fried M, Schölmerich J, Obermeier F and Rogler G. BCL-2 modifying factor (BMF) is a central regulator of anoikis in human intestinal epithelial cells. J Biol Chem 2011; 286: 26533-26540.
[29] Cirillo N, Lanza M, De Rosa A, Cammarota M, La Gatta A, Gombos F and Lanza A. The most widespread desmosomal cadherin, desmoglein 2, is a novel target of caspase 3-mediated apoptotic machinery. J Cell Biochem 2008; 103: 598-606.
[30] Yang T, Gu X, Jia L, Guo J, Tang Q, Zhu J, Zhao W and Feng Z. DSG2 expression is low in colon cancer and correlates with poor survival. BMC Gastroenterol 2021; 21: 7.
[31] Zou Y, Xu L, Wang W, Zhu X, Lin J, Li H, Chen J, Xu W, Gao H, Wu X, Yin Z and Wang Q. Muscone restores anoikis sensitivity in TMZ-resis-

tant glioblastoma cells by suppressing TOP2A via the EGFR/Integrin β1/FAK signaling pathway. Phytomedicine 2024; 129: 155714.
[32] Alanko J, Mai A, Jacquemet G, Schauer K, Kaukonen R, Saari M, Goud B and Ivaska J. Integrin endosomal signalling suppresses anoikis. Nat Cell Biol 2015; 17: 1412-1421.
[33] Chen N and Debnath J. IκB kinase complex (IKK) triggers detachment-induced autophagy in mammary epithelial cells independently of the PI3K-AKT-MTORC1 pathway. Autophagy 2013; 9: 1214-1227.
[34] Wu X, Li S, Wang K, Hua W, Li S, Song Y, Zhang Y, Yang S and Yang C. TNF-α regulates ITGβ1 and SYND4 expression in nucleus pulposus cells: activation of FAK/PI3K signaling. Inflammation 2019; 42: 1575-1584.
[35] Marconi A, Atzei P, Panza C, Fila C, Tiberio R, Truzzi F, Wachter T, Leverkus M and Pincelli C. FLICE/caspase-8 activation triggers anoikis induced by beta1-integrin blockade in human keratinocytes. J Cell Sci 2004; 117: 5815-5823.
[36] Guha D, Saha T, Bose S, Chakraborty S, Dhar S, Khan P, Adhikary A, Das T and Sa G. Integrin-EGFR interaction regulates anoikis resistance in colon cancer cells. Apoptosis 2019; 24: 958-971.
[37] Giusti B, Margheri F, Rossi L, Lapini I, Magi A, Serratì S, Chillà A, Laurenzana A, Magnelli L, Calorini L, Bianchini F, Fibbi G, Abbate R and Del Rosso M. Desmoglein-2-integrin Beta-8 interaction regulates actin assembly in endothelial cells: deregulation in systemic sclerosis. PLoS One 2013; 8: e68117.
[38] Lorch JH, Thomas TO and Schmoll HJ. Bortezomib inhibits cell-cell adhesion and cell migration and enhances epidermal growth factor receptor inhibitor-induced cell death in squamous cell cancer. Cancer Res 2007; 67: 727-734.

Supplementary Table 1. QPCR Primer sequences and the siRNA interference sequences and the DSG2 overexpression sequences

Gene	Forward Primer (5'-3')	Reverse Primer (5'-3')
DSG2	CTAACAGGTTACGCTTTGGATGC	GTGAACACTGGTTCGTTGTCAT
GAPDH	CTGGGCTACACTGAGCACC	AAGTGGTCGTTGAGGGCAATG
Gene	SS Sequence	AS Sequence
SiNC	AAUUCUCCGAACGUGUCACGU	ACGUGACAGGUUCGGAGAAUU
SiDSG2-1	GGAUGUCAAUGACAAUAUACC	UAUAUUGUCAUUGACAUCCAA
SiDSG2-2	GGAAGUAGAUUAUGAAGAAAU	UUCUUCAUAAUCUACUUCCUU
SiDSG2-3	CAGUGUUCUACCUAAAUAAAG	UUAUUUAGGUAGAACACUGGA
Gene	Primer sequence (5'-3')	
pcDNA3.1-DSG2-F	TACCGAGCTCGGATCCGCCACCATGGCGCGGAGCCCGGGACG	
pcDNA3.1-DSG2-R	GATATCTGCAGAATTCTTAGGAGTAAGAATGCTGTAC	

Supplementary Table 2. Antibody information used in this study

Gene name	Manufacturer	Article number	Dilution ratio
DSG2	Affinity	DF3988	1:1000
Integrin β1	Affinity	AF5379	1:1000
p-Integrin β1	Affinity	AF8384	1:1000
FAK	Affinity	AF6397	1:1000
p-FAK	Affinity	AF3398	1:1000
P53	abcam	ab26	2 μg/ml
Bcl-2	abcam	ab182858	1:2000
Bax	abcam	ab32503	1:1000
Caspase-3	abcam	ab32351	1:5000
Cleaved-Caspase-3	Affinity	AF7022	1:1000
GAPDH	HUABio	ER1901-65	1:1000
Alexa Fluor® 488	ZSBio	ZF-0511	1:200
Alexa Fluor® 594	ZSBio	ZF-0516	1:200
Goat Anti-Rabbit IgG H&L (HRP)	Bioss	bs-40295G-IRDye8	1:10000
Goat Anti-Mouse IgG H&L (HRP)	Bioss	bs-0296G-AP	1:1000

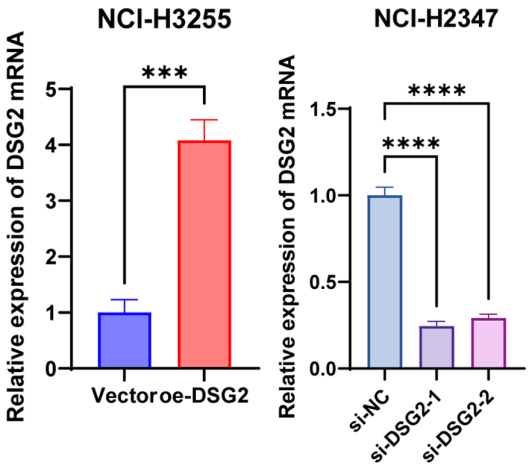

Supplementary Figure 1. Construction of DSG2 over - expression and knockdown cell models. In NCI-H3255 cells, the DSG2 over-expression plasmid was transfected and incubated for 48 hours to construct a DSG2 over-expression cell model. In NCI-H2347 cells, si-DSG2-1 and si-DSG2-2 interfering RNAs were transfected and incubated for 48 hours. After the incubation, the relative expression level of DSG2 mRNA was detected by RT-qPCR assay (* indicates a statistically significant difference between the two groups, ***P < 0.001, ****P < 0.0001).